19th Australasian Fluid Mechanics Conference
Melbourne, Australia
8-11 December 2014

Microbubble Content in the Wake of a Cavitating Hydrofoil

K. L. de Graaf, G. A. Zarruk, P. A. Brandner and B. W. Pearce

Australian Maritime College,
University of Tasmania, Launceston, Tasmania 7250, Australia

Abstract

The microbubble content in the wake of a cavitating hydrofoil is investigated in a variable pressure water tunnel using long-range microscopy shadowgraphy. A 200 mm span, 120 mm base-chord NACA 63A015 section elliptical planform hydrofoil was mounted at 3.5° incidence in a 0.6 m square tunnel test section. The microbubbles generated by the cavitation in the hydrofoil wake at a Reynolds number of 0.5×10^6 and a cavitation number of 0.37 were characterised at several locations. The bubble content was photographed at three locations downstream of the trailing edge, and five spanwise and three transverse locations. Measurements were made downstream of the region where shed vortices from the cavity trailing edge are still visible. The bubbles were back-lit using diffused laser lighting and images captured with a CCD camera. The image resolution was approximately 2 µm/pixel. The dominant bubble size in the wake was found to range between 25 and 40 µm depending on location. Bubbles larger than 200 µm are evident in the wake but not well captured with these tests. Additional tests with a higher magnification are required to image bubbles below 20 µm.

Introduction

The characteristics of propeller induced wakes are important for the development of acoustic scattering models for surface and sub-sea vehicles. This requires an understanding of the basic physical properties, processes and interactions that control bubble size and distribution in the near field of a rotating propeller. Data are required for determining the initial conditions for computational fluid dynamics modelling of the structure and evolution of these bubble distributions within the propeller wake. To gain understanding of the flow field and bubbly flow about a propeller, a hydrofoil may be used as a simplified geometry capable of generating similar underlying physics. A hydrofoil also allows data collection at higher Reynolds numbers unachievable with a propeller in water tunnel experiments.

There is scant information on the microbubble size and distribution in the wake of a hydrofoil. Maeda *et al.* [6] used holography to measure the bubble distribution in cloud cavitation about a hydrofoil and found the dominant bubble size to be in the order of 10 - 20 µm. Yu and Ceccio [8] using holography also found a dominant bubble size of 10 - 20 µm in the wake of a partial cavity. Qin *et al.* [7] used Phase Doppler Anemometry to measure bubbles in the wake of a NACA 0015 hydrofoil and found the average bubble size to be 250 µm. Lee *et al.* [5] made shadowgraphy measurements in the wake of a ventilated NACA 0015 hydrofoil and found the dominant bubble size to be about 200 µm. From the above it is evident that little is known about the underlying physics governing the bubble size and distribution in the wake of a propeller or hydrofoil.

This paper presents results from flow visualization experiments using long-range microscopy shadowgraphy and high resolution imaging to estimate the microbubble size and distribution in the wake of an elliptical planform hydrofoil.

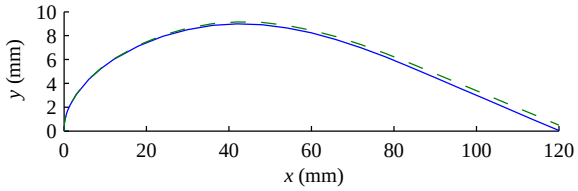

Figure 1. Comparison of standard and modified NACA 63A015 section. Standard profile blue solid line, modified profile green dashed line.

Experimental Setup and Methods

A 200 mm span, 120 mm base-chord aluminium hydrofoil of elliptical planform with a modified NACA 63A015 section was manufactured and mounted from the ceiling in the test section of the Cavitation Research Laboratory (CRL) variable-pressure water tunnel at the University of Tasmania. The hydrofoil was modified to have a thicker trailing edge to reduce susceptibility to damage. The modified profile was achieved by adding $0.00385x$ to the standard profile equation, giving:

$$y = 0.12\sqrt{1.65^2 - \left(\frac{x}{0.12} - 1.65\right)^2} + 0.00385x \qquad (1)$$

where y is the offset at the chordwise location x. The profiles are shown in figure 1.

The test section of the tunnel is 0.6 m square and 2.6 m in length. The tunnel velocity can be varied from 2 - 12 m/s and the centreline pressure from 4 - 400 kPa (absolute). Further details on the tunnel and facility can be found in [1, 2]. The hydrofoil was set at an incidence, α, of 3.5° and the free stream velocity was set to give a chord-based Reynolds number, Re_c, of 0.5×10^6. The cavitation number, $\sigma = (p - p_v)/(1/2\rho U^2)$, where p is the pressure in the centreline of the tunnel, p_v the vapour pressure, ρ the density of the fluid, and U the mean freestream velocity, was set at 0.37.

Forward-lit photographs were taken of the cavitating hydrofoil to capture the extent and macroscopic bubble distribution of the wake. These were obtained with a Canon 50D 35 mm SLR camera and Canon EF 24-70 mm lens with triggered stroboscopic lighting (DRELLO 1018/LE4040).

Shadowgraphy measurements were made in the bubbly wake of the hydrofoil, downstream of the region in which hairpin vortex shedding is visible (see figures 2 - 3). Several locations were sampled to investigate the microbubble distribution in the streamwise, spanwise and transverse planes. These locations are summarised in table 1 and figure 2. The distances from the hydrofoil mid-chord axis to the sampled locations in the streamwise, d_d, and transverse, d_o, directions are non-dimensionalised using the hydrofoil chord, c. The distance in the spanwise, d_s, direction from the root is non-dimensinoalised using the span, s. A positive offset from the hydrofoil mid-chord axis is towards the pressure side or into the page as shown in figure 2. One thousand images were taken at each location to obtain converged statistics [3]. The shadow photographs were backlit using a 120

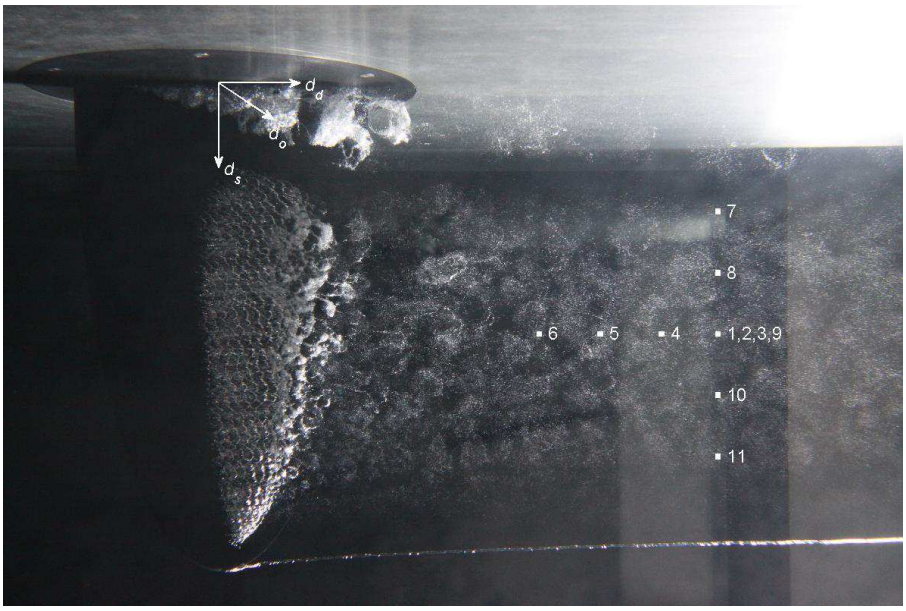

Figure 2. Image showing the 11 locations sampled in the wake of the cavitating hydrofoil. The cavitating root and tip vortices limit the spanwise extent of the sheet cavitation that condenses/collapses producing microbubbles that seed the wake. The sheet cavitation initially breaks down to cavitating vortices that further condense to remnant microbubbles of incondensable gas with apparent clustering of the scale of the vortical structures. α = 3.5°; $Re_c = 5\times10^6$, σ = 0.37.

Location #	d_d/c	d_o/c	d_s/s
1	1.708	0.0175	0.500
2	1.708	0.0590	0.500
3	1.708	-0.0240	0.500
4	1.500	-0.0050	0.500
5	1.292	-0.0050	0.500
6	1.083	-0.0050	0.500
7	1.708	-0.0050	0.250
8	1.708	-0.0050	0.375
9	1.708	-0.0050	0.500
10	1.708	-0.0050	0.625
11	1.708	-0.0050	0.750

Table 1. Summary of sampled locations.

mJ Litron Nano L PIV Nd:YAG laser diffused through a LaVision high efficiency diffuser. The emitted light pulses are in the wavelength range 574 to 580 nm and of 20 ns duration when excited by the 532 nm wavelength laser pulses of 5 ns duration. A Lavision Imager Intense camera with a Questar QM1 long-range microscope captured images at 4.5 Hz of size 1376×1040 pixels. The field of view of the camera was 2.94×2.22 mm giving a resolution of about 2 µm/pixel. Assuming that a minimum resolution of 10 pixels across the diameter is required for bubble sizing [3], this configuration gave an expected lower limit on bubble identification of 20 µm diameter. Triggering of the laser and camera and analysis of the shadow images was done using LaVision DaVis software version 8.1.

Results

Forward-lit images of the cavitating hydrofoil are shown in figures 2 - 4. The general structure is evident, with the spanwise extent of the sheet cavity limited by root and tip vortices. The periodic spanwise features on the sheet cavity surface are due to Kelvin-Helmholtz instabilities in the overlying separating boundary layer. These instabilities lead to break up of the cavity trailing edge with hairpin vortex formation. Further downstream the structures condense leaving populations of microbubbles in clusters of a length scale similar to the shed vortices. The present work is focused on analysis and determination of the size distribution of the microbubble population in this region of the wake. Figure 5 shows an example shadowgraph image taken of the wake at location 7.

Using this shadowgraph technique, the relevant sample volume for each detected bubble varies. To calculate statistically significant results, two corrections are made to the detection probability of each bubble, the depth of field correction: $p_{i,DOF} = D_i/D_{Reference}$, and the border correction, $p_{i,Border} = (W - D_i)(H - D_i)/WH$, where D_i is the particle diameter, $D_{Reference}$ is the reference diameter, W is the field of view width and H is the field of view height [4].

Figures 6 - 8 show the volumetric concentration, V_C, void fraction, V_f, and dominant bubble size, D_{dom}, for the streamwise, spanwise and transverse planes in the wake of the hydrofoil. The volumetric concentration, dominant bubble size, and void fraction (though only marginally) were found to decrease with increased distance downstream of the hydrofoil (figure 6). A decrease in dominant bubble size suggests dissolution or condensation, or possible dispersion of larger bubbles. It could also suggest bubble breakup; however, this far downstream of the hydrofoil it is unlikely that the turbulence is strong enough for this to occur. Bubble dissolution and condensation would also result in a reduced void fraction, as seen here. The decrease in volumetric concentration suggests bubble dispersion due to turbulence in the wake (see figure 4) or possible coalesence. In this case, as the dominant bubble size is also decreasing, it is unlikely that the bubbles are undergoing significant coalescence. From the three properties, it can be deduced that the bubbles are undergoing dissolution or condensation and some dispersion.

The volumetric concentration was also found to decrease at the upper and lower edges of the wake (figure 7). This is expected as the bubbles disperse and mix with the outer unseeded flow. Again, this is reflected in the decreased void fraction at these locations. The dominant bubble size in the spanwise plane varies. Larger bubble sizes towards the edge suggest they may be more

Figure 3. Enlarged section of figure 2. The periodic spanwise features on the sheet cavity surface are due to Kelvin-Helmholtz instabilities in the overlying separating boundary layer. These instabilities lead to break up of the cavity trailing edge with hairpin vortex formation.

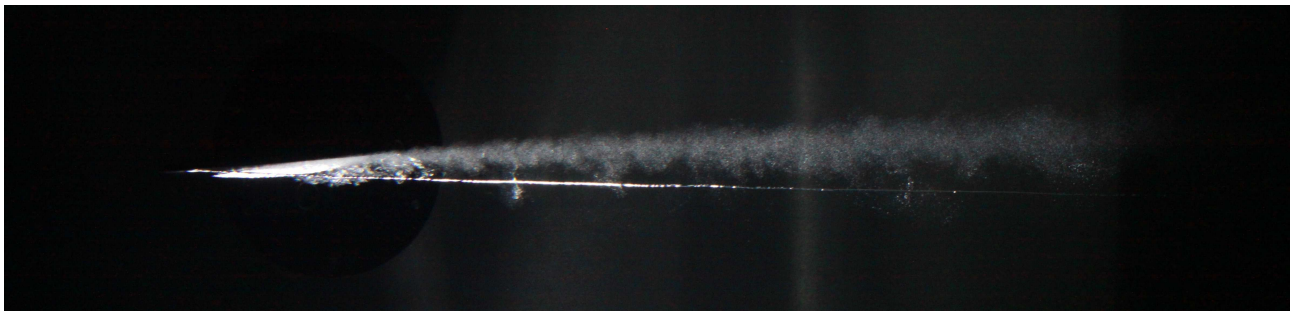

Figure 4. Hydrofoil wake from underneath showing cavitating tip vortex and bubbly wake from break down of sheet cavitation. $\alpha = 3.5^\circ$; $Re_c = 5\times10^6$, $\sigma = 0.37$.

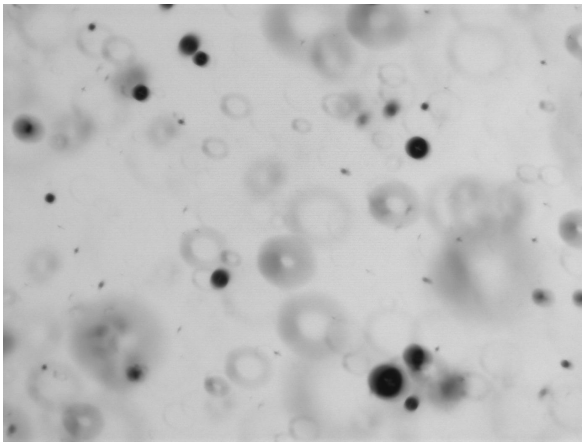

Figure 5. Sample image taken of the wake at a downstream location of $d_d/c = 1.708$ and a spanwise location of $d_s/s = 0.25$ (location 7).

easily convected by the turbulent flow, which is in keeping with the suggestion of dispersion of larger bubbles with increased distance downstream. Across the wake (figure 8), the volumetric concentration and void fraction again decrease towards the transverse extents as the bubble population mixes out.

Figures 9 and 10 show sample bubble size distributions. Across all of the locations, the dominant bubble size ranges from 25 to 40 µm. For locations where the dominant bubble size is 25 µm, it is likely that the dominant size may be smaller than this and that the spectra is not fully resolved. It was found that the minimum accurately detectable bubbles were between 30 and 40 µm. This corresponds to requiring a minimum of 15 - 20 pixels across the bubble diameter, not the assumed 10 pixels. As the bubbles appear to be generally smaller than 40 µm in diameter, further work with improved optics is required to fully characterise the microbubble size distribution.

In addition to increasing the magnification and/or resolution to obtain a more accurate determination of the size distribution, information on spatial distribution and clustering phenomena would also be of interest. This can be obtained with optical techniques that possess high spatial resolution such as Interferometric Mie Imaging (IMI) or time-resolved shadowgraphy.

Conclusions

Preliminary shadowgraph images were taken of the cavitating wake of an elliptical planform, modified NACA 63A015 section hydrofoil of 200 mm span and 120 mm base-chord at $\alpha = 3.5^\circ$, $Re_c = 0.5 \times 10^6$, and $\sigma = 0.37$. The bubble size distribution is similar across the locations sampled and shows a dominant bubble size of 25 to 40 µm. As this is at the lower limit of resolution for the current optics, further measurements with improved resolution are required, in addition to a much denser matrix of sample locations, to capture the entire size range of detectable bubbles and resolve the bubble size distribution.

Acknowledgements

The authors wish to acknowledge the support of the University of Tasmania and the Defence Science and Technology Organisation (Mr. Brendon Anderson, Dr. Richard Ellem and Dr. Alexei Kouzoubov).

References

[1] Brandner, P. A., Lecoffre, Y. and Walker, G. J., Development of an Australian national facility for cavitation research, in *6th International Symposium on Cavitation*, Wageningen, The Netherlands, 2006.

[2] Brandner, P. A., Lecoffre, Y. and Walker, G. J., Design considerations in the development of a modern cavitation tunnel, in *16th Australasian Fluid Mechanics Conference*, Gold Coast, Australia, 2007, 630–637.

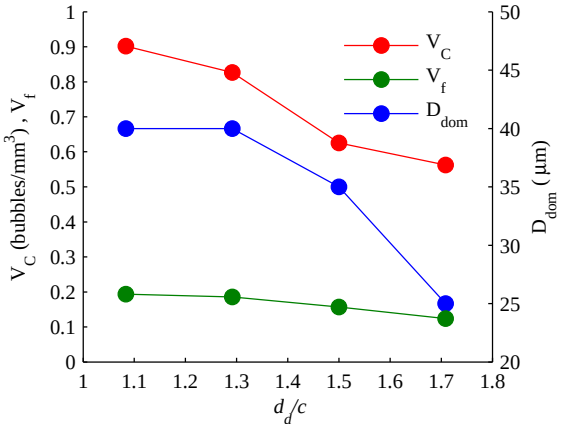

Figure 6. Bubble statistics downstream of hydrofoil showing volumetric concentration, V_C, void fraction, V_f, and dominant bubble size, D_{dom}, at locations 6, 5, 4 and 9.

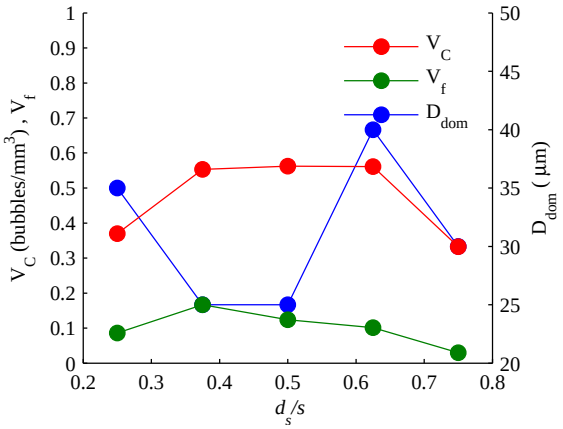

Figure 7. Bubble statistics downstream of hydrofoil in the spanwise plane showing volumetric concentration, V_C, void fraction, V_f, and dominant bubble size, D_{dom}, at locations 7, 8, 9, 10 and 11.

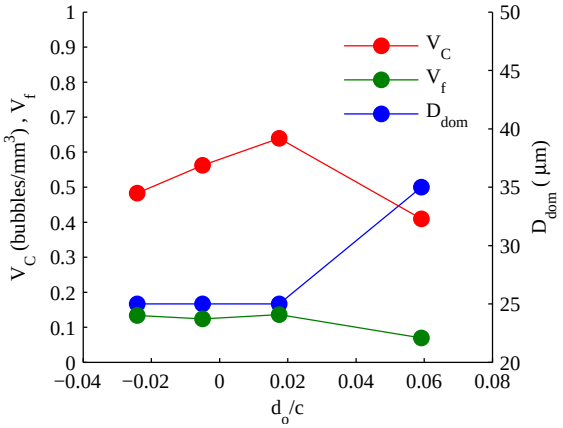

Figure 8. Bubble statistics downstream of hydrofoil in the transverse plane showing volumetric concentration, V_C, void fraction, V_f, and dominant bubble size, D_{dom}, at locations 3, 9, 1 and 2.

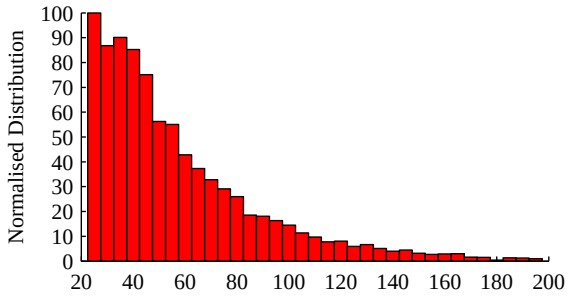

Figure 9. Bubble size distribution (location 1).

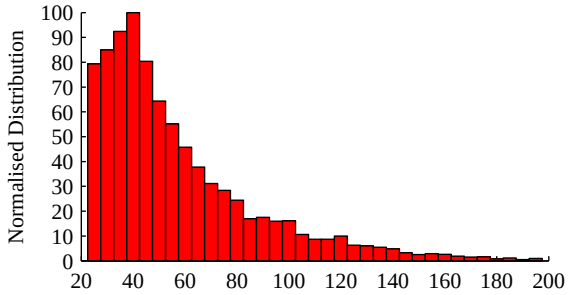

Figure 10. Bubble size distribution (location 5).

[3] Brandner, P. A., Wright, G., Pearce, B., Goldsworthy, L. and Walker, G. J., An experimental investigation of microbubble generation in a confined turbulent jet, in *17th Australasian Fluid Mechanics Conference*, Auckland, New Zealand, 2010, Paper 292.

[4] LaVision, *ParticleMaster Shadow Product-Manual 1105032*, LaVision, Göttingen, Germany, 2008.

[5] Lee, S. J., Kawakami, E. and Arndt, R. E. A., Measurements in the wake of a ventilated hydrofoil, in *Proceedings of ASME 2013 Fluids Engineering Division Summer Meeting*, Incline Village, USA, 2013.

[6] Maeda, M., Yamaguchi, H. and Kato, H., Laser holography measurement of bubble population in cavitation cloud on a foil section, in *FED-Vol. 116 Cavitation*, 1991, 67–75.

[7] Qin, Q., Wang, H. and Arndt, R. E. A., An integrated experimental/numerical study of the bubble wake behind a cavitating hydrofoil, in *Proceedings ASME 2005 Fluids Engineering Division Summer Meeting*, Houston, USA, 2005.

[8] Yu, P.-W. and Ceccio, S. L., Diffusion induced bubble populations downstream of a partial cavity, *Journal of Fluids Engineering*, **119**, 1997, 782–787.